IEEE Access
Multidisciplinary ⋮ Rapid Review ⋮ Open Access Journal

Received August 2, 2021, accepted August 23, 2021, date of publication August 24, 2021, date of current version August 31, 2021.

Digital Object Identifier 10.1109/ACCESS.2021.3107631

Maximal Selective Transmit Diversity for Petahertz Wireless Communications With Continuous Waveform Detector

SUDHANSHU ARYA[1], (Member, IEEE), AND YEON HO CHUNG[2], (Senior Member, IEEE)
[1]Department of Artificial Intelligence Convergence, Pukyong National University, Busan 48513, Republic of Korea
[2]Department of Information and Communications Engineering, Pukyong National University, Busan 48513, Republic of Korea

Corresponding author: Yeon Ho Chung (yhchung@pknu.ac.kr)

This work was supported by the Basic Science Research Program through the National Research Foundation of Korea (NRF) funded by the Ministry of Education under Grant 2018R1D1A3B07049858.

ABSTRACT Motivated by unique atmospheric scattering properties of optical waves at petahertz frequencies, we present a novel maximal selective transmit diversity scheme based on the selection of maximum irradiance optical path with a continuous waveform detector employed for petahertz wireless communications. The proposed scheme is designed to significantly improve the performance of a non-line-of-sight (NLOS) petahertz link in a turbulence-induced fading channel. We characterize the received signal by a continuous wave detector and quantify the cumulative distribution function (CDF) of the largest order statistics of the received irradiance. Furthermore, we derive closed-form expressions of important performance metrics including the average bit error rate, the outage probability, and the optical channel capacity with each scattered path experiencing the Gamma-Gamma distributed turbulence-induced fading. From the analytical expressions derived, the performance of the proposed NLOS petahertz communication system is analyzed and validated. Simulation results show that the proposed scheme effectively overcomes the channel impairment without increasing the transmit power. Even under strong turbulence fading, when the number of transmit diversity branches increases from 1 to 2 and 4, the required average signal-to-noise ratio (SNR) to maintain an outage probability of 10^{-5} is found to be significantly reduced by 13 dB and 21 dB, respectively.

INDEX TERMS Average bit error rate, continuous waveform detector, free-space optical communications, optical channel capacity, outage probability, petahertz communications, transmit diversity.

I. INTRODUCTION

The desire for low-cost, high-speed, and low-power communication links has motivated recent interest in optical wireless communications (OWC). Infrared (IR) and visible light communication (VLC) based OWC systems have been extensively used in indoor and outdoor optical communication applications through line-of-sight and diffused links.

The conventional OWC employing IR or VLC is a promising technology capable of offering high data rate. However, these links are always susceptible to blockage due to their strict requirement of pointing, acquisition, and tracking (PAT). Furthermore, atmospheric turbulence produces fluctuations in the irradiance of the received beam, thereby severely degrading the communication performance. Various performance improvement techniques have been reported to address the performance impairments in the conventional OWC systems. A performance enhancement scheme for a wavelength division multiplexing for the OWC channel impaired by interchannel crosstalk, pointing error, and amplified spontaneous emission was reported [1]. The receiver sensitivity over the turbulence channel was shown to improve significantly by utilizing spatial modulation and pulse position modulation. Another interesting technique by the same authors to improve the performance of an orbital angular momentum-based multiplexed link over the OWC channel was documented [2]. An adaptive multiple-input-multiple-output OWC link with spatial multiplexing was proposed

The associate editor coordinating the review of this manuscript and approving it for publication was Adnan M. Abu-Mahfouz.

for OAM-based optical communication. It was shown that the channel capacity was increased significantly. A hybrid technique employing mode division multiplexing and orthogonal frequency division multiplexing for free-space optical communications over Gamma-Gamma distributed turbulence channel was presented [3]. The authors considered the Hermite Gaussian modes and investigate the performance under the beam divergence. A 1-bit feedback-based beamforming scheme for OWC based non-orthogonal multiple access system was reported for negative exponentially distributed turbulence fading. It was demonstrated analytically that the system suppresses the error due to the successive interference cancellation [4].

In contrast to IR and VLC links, a high degree of relatively angle-independent Rayleigh and Mie scattering in the petahertz frequency band makes it an appropriate choice for non-line-of-sight (NLOS) optical communication links [5]. The petahertz communication, therefore, eliminates the PAT requirement and accommodates NLOS link capabilities. In addition, within the entire petahertz band, the ultraviolet-C (UV-C) band with wavelengths ranging from 200 to 280 nm has lower solar background noise because of the ozone filtering at the upper atmosphere [6].

Reflecting this keen interest in the UV feature, there have been considerate efforts in developing and designing a UV communication system for indoor and outdoor applications [7]–[10]. A single scattering UV channel modeling was proposed [11]. This channel modeling, based on the prolate-spheroidal coordinate system with coplanar geometry, described the temporal characteristics of the NLOS UV link. A simplified closed-form single-scattering NLOS UV channel modeling was documented [12]. In [13], a log-normal distributed turbulence channel modeling for a short range UV link was presented. The atmospheric turbulence fading is one of the main channel impairments affecting the performance of the UV communication links. It results in rapid fluctuations in the received optical beams. While atmospheric turbulence fading can generally be ignored for relatively smaller propagation distances and clear atmospheric conditions, it degrades the performance as propagation distance is extended.

Though UV spectrum has important properties such as solar blindness in the UV-C band and high atmospheric absorption and scattering which enables NLOS communication, the strong scattering results in a temporal dispersion of the transmitted UV pulses, thereby resulting in intersymbol interference (ISI) with a low received signal-to-noise ratio (SNR). This low received SNR with ISI may result in high error rate [14]. As a method for improving the bit error rate, an interesting count-and-forward relaying communication system was reported with an optimal solution to the power optimization [15]. It was also demonstrated that under scattering channel, the scheme outperforms the relay schemes based on the hard-decision. In [16], a UV based dual-hop cooperative communication system employing orthogonal frequency-division multiplexing over a deterministic channel was reported. Interestingly, this work exhibited a significant improvement in error rate performance over point-to-point communications.

In addition to the fundamental drawbacks including ISI and high path loss, the performance is prone to the atmospheric turbulence. To overcome these limitations, a relay-assisted amplify-and-forward NLOS UV communication system under gamma-gamma distributed turbulence fading was proposed [17]. The authors derived the exact solution for the optimal number of relay. In addition, the closed-form expressions for the outage probability, error rate, and channel capacity were derived. A decode-and-forward relay-based UV system over log-normal distributed turbulence fading was presented [18]. For this relay scheme, the authors also derived the closed-form expression for the outage probability and also quantified the diversity gain as a function of the UV channel parameters and link geometry. Another UV based cooperative communication system based on the best relay selection algorithm was considered with the decode-and-forward relaying protocol [19]. The authors analyzed the outage probability under log-normal distributed turbulence fading. The widely reported turbulence model in the literature for UV communication is based on the log-normal distribution. However, it is only valid under weak turbulence fading [20]–[22]. As the propagation path increases to several kilometers, the channel tends to undergo strong turbulence fading, thereby making log-normal distribution invalid in channel modeling [23]. Under a strong turbulence regime, the gamma-gamma distribution has been experimentally proved valid with distribution parameters directly related to atmospheric conditions [24].

In [9], we proposed a spatial receive diversity technique for improving the performance of the NLOS UV links, where the switch-and-stay diversity was utilized at the receiver to lower the outage probability in the gamma-gamma distributed turbulence channel. We also analyzed the effect of the receiver correlation. It was demonstrated that the scheme has an optimal performance when there is no correlation; however, the performance degrades as the correlation increases.

In this paper, we consider a transmit diversity scheme which exploits the fact that the turbulence-induced fading in an optical channel is slow time-varying fading [25]. The proposed scheme is based on selecting the optical path at the transmitter with a higher value of the irradiance. A key novelty of this work is that, unlike previous UV studies, a combined consideration of slow-fading UV channel with transmit diversity is given to improve the performance of the NLOS UV links. This paper considers the gamma-gamma distributed turbulence fading. We derive the marginal probability density function (PDF) of the received UV signal with the maximum value of the irradiance, considering the NLOS geometry.

A. CONTRIBUTIONS

The novel contributions of this manuscript are listed as follows:

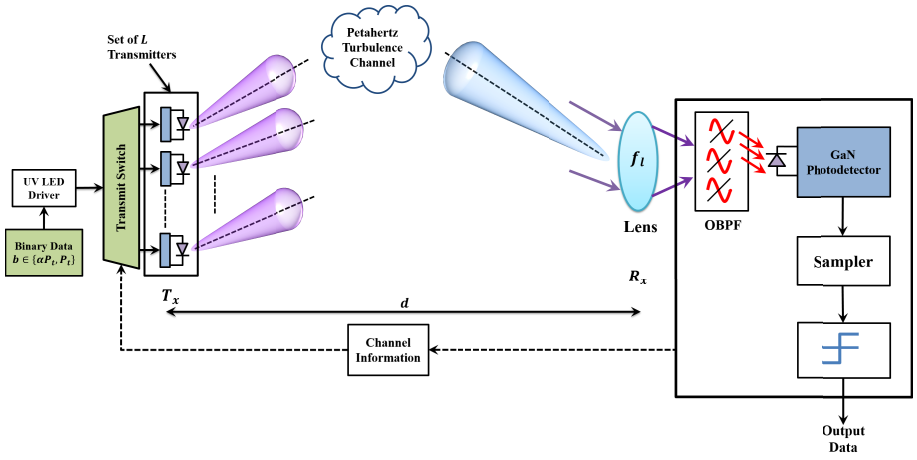

FIGURE 1. System model.

- We consider petahertz wireless scattering communication and characterize the received signal by a continuous waveform detector. Given that the turbulence-induced fading is a slow time process and assuming the channel information at the transmitter, we quantify the CDF of the largest order statistics of the received irradiance.
- Considering the maximal selection transmit diversity for scattering communications, a mathematical tractable expression for the average bit error rate is derived.
- The closed-form expression for the marginal PDF of the instantaneous received SNR is derived. Subsequently, the closed-form expression for the outage probability is obtained.
- Considering the non-ergodic slow-fading turbulence channel, the closed-form expression for the optical channel capacity for the given channel conditions is derived.
- All the derived expressions are validated by analyzing the performance of the proposed system. It is shown that the performance of the maximal selection transmit diversity technique outperforms the repetition codes and orthogonal space-time-block codes techniques.

The rest of the paper is organized as follows. Section II presents the system model. Section III gives an analytical approach to evaluate the average bit error rate, outage probability, and optical channel capacity. Results and discussions are given in Section IV, and conclusions are drawn in Section V.

II. SYSTEM MODEL: CONTINUOUS WAVE DETECTOR

The proposed system model is illustrated in Fig. 1. We consider multiple-input single-output maximal selection transmit diversity with L diversity branches. The intensity-modulation with direct detection (IM/DD) on-off keying (OOK) transmission scheme is utilized. We assume non-return-to-zero pulse formats for OOK modulated signal. The binary data $b \in \{\alpha P_t, P_t\}$ is the signal level for the data symbol

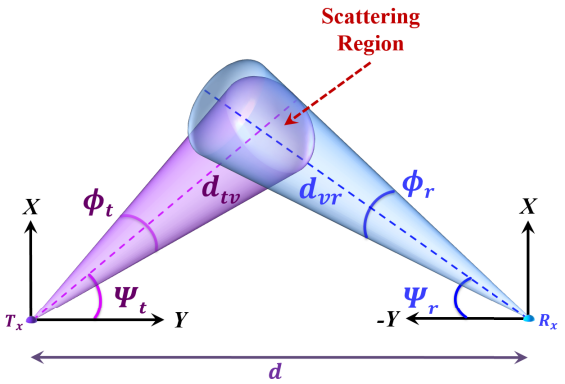

FIGURE 2. Illustration of the NLOS scattered link in petahertz wireless communication.

corresponding to the information bit 0 and 1. α is the optical source extinction ratio, such that $0 \leq \alpha < 1$.

The UV scattered light that reaches the receiver depends on the link geometry and the optical characteristics of the atmosphere. Fig. 2 illustrates a typical NLOS UV communication link. The transmitter and the receiver are separated by a baseline distance d. ϕ_t and ϕ_r are the transmitter beam full-width divergence angle and the receiver field-of-view (FOV), respectively. ψ_t and ψ_r denote the transmitter and the receiver elevation angle, respectively. The distances of the intersected (overlap) common volume V_c to the transmitter and the receiver are represented by d_{tv} and d_{vr}, respectively. θ_s is the scattering angle and is given by $\theta_s = \psi_t + \psi_r$.

The instantaneous received signal $y(t)$ suffers from a fluctuation in signal intensity due to atmospheric turbulence and can be well modeled as

$$y(t) = SHP_t(t)I(t) + w(t), \tag{1}$$

where S is the receiver responsivity in A/W. Since the IM/DD transmission scheme with OOK modulation is utilized, the transmitted information bit is either 0 or P_t, where

$P_t/2$ is the average transmitted optical power. I denotes the scintillation at the optical path and describes the strength of turbulence. H is the channel state and is given by $H = h_t \times h_l \times h_g$, where $\times$ denotes the multiplication operator. h_t is the attenuation term due to atmospheric turbulence given by [18]

$$h_t = 10^{-\frac{\sqrt{23.17C_n^2k^{7/6}}\left(\sqrt{d_{tv}^{11/6}+d_{vr}^{11/6}}\right)}{5}}. \tag{2}$$

where C_n^2 represent the index of refraction structure parameter of the atmosphere. It is used as a measure of the turbulence strength and typically varies from 10^{-13} to 10^{-17} $m^{-2/3}$ [23]. $k = 2\pi/\lambda$ denotes the optical wave number where λ is the wavelength of the optical signal.

h_l is the attenuation due to path loss and is a deterministic quantity given by [26]

$$h_l = \frac{A_r\alpha_s q_s \phi_t^2 \phi_r \sin\theta_s \left(12\sin^2\psi_r + \phi_r^2\sin^2\psi_t\right)}{96d\sin\psi_t\sin^2\psi_r\left(1-\cos\frac{\phi_t}{2}\right)\exp\left[\frac{\alpha_t d(\sin\psi_t+\sin\psi_r)}{\sin\theta_s}\right]}, \tag{3}$$

where A_r denotes the effective area of the receiver and q_s is the scattering phase function and is modeled as a combination of Rayleigh and Mie scattering phase function [26]. α_s is the total scattering coefficient and is defined as the sum of the Rayleigh and Mie scattering coefficients. α_t denotes the total extinction coefficient and is given by the sum of the scattering and absorption coefficients as $\alpha_t = \alpha_s + \alpha_a$. h_g represents the loss due to the geometric spreading.

$w(t)$ denotes the additive white Gaussian noise (AWGN) with noise variance N_0 which is equal to the AWGN noise power. Considering the additive white Gaussian noise from both the detector thermal noise and the background radiation, $w(t)$ satisfies the following distribution [27], [28]

$$w \sim \mathcal{N}(0, \sigma_{DC}^2 + \sigma_T^2), \tag{4}$$

where $\sigma_{DC}^2 = 2Q_eI_{DC}B$ is the variance of the zero-mean shot noise due to the background radiation and $\sigma_T^2 = \frac{2kT_e}{R_L}T_s$ is the variance due to the thermal noise. Q_e is the electronic charge, I_{DC} is the dark current due to background illumination, and B denotes the bandwidth of the detector. k is the Boltzmann constant, R_L is the load resistance, and T_e is the temperature. T_s denotes the symbol duration. It is to be noted that, since the shot and thermal noises are independent random processes that can be modeled using Gaussian statistics, the total variance N_0 can simply be obtained by adding the individual variances, as illustrated in (4).

A. BACKGROUND

1) ATMOSPHERIC SCINTILLATION

The atmospheric channel is composed of air molecules, aerosols, dust, water vapor, and pollutants with a size comparable to the wavelength of a typical optical signal, thereby resulting in an atmospheric absorption and scattering which significantly attenuate the transmitted optical signal. On the other hand, inhomogeneities induced by the atmospheric temperature and pressure result in scintillation. It causes a deleterious impact on the performance of free-space optical communication systems [29]. Scintillation is caused by atmospheric turbulence which induces fluctuations in the amplitude and phase of the received optical signal intensity [28]. Therefore, this turbulence-induced fading can be a limiting factor in reliable optical wireless communication link performance. The effects of atmospheric turbulence on the propagation of an optical wave can be characterized by the Rytov variance defined as

$$\sigma_R^2 = 1.23C_n^2k^{7/6}d_{TR}^{11/6}, \tag{5}$$

where C_n^2 and k are defined in (2). In terms of σ_R^2, the turbulence strength can be characterized as weak atmospheric turbulence by the condition $\sigma_R^2 < 1$ and moderate-to-strong turbulence by $\sigma_R^2 > 1$. d_{TR} denotes the propagation distance of an optical beam.

2) GEOMETRICAL SPREADING

Geometric spreading of the transmitted optical beam adversely affects the performance at the receiver side. To quantify the impairment caused by the geometric spreading of the optical beam, consider a Gaussian beam profile with a photodetector of radius R_D. The conditional normalized spatial distribution of the beam scattered at the common volume at any distance d_{vr} from the common volume can then be formulated as [30]

$$U_{beam}(\rho; d_{vr}|\, d_{tv}) = \frac{2}{\pi w_{d_{vr}}^2}\exp\left(-\frac{2\|\rho\|^2}{w_{d_{vr}}^2}\right), \tag{6}$$

where ρ represents the radial vector measured from the scattered beam center. $w_{d_{vr}}$ denotes the waist of the scattered beam after traversing a distance d_{vr} measured from the scattering center. The loss in the received power due to geometric spreading can be calculated as

$$h_g(r_{bc}; d_{vr}) = \int_{A_D} U_{beam}(\rho - r_{bc}; d_{vr}|\, d_{tv}), \tag{7}$$

where A_D represents the area of the detector and r_{bc} is the beam center.

3) MARGINAL DISTRIBUTION OF THE RECEIVED SCATTERED SIGNAL

As depicted in the previous subsection, to describe the geometric spreading, we consider a Gaussian beam profile. The propagation of the Gaussian beam over the turbulence channel can be best analyzed using the Gamma-Gamma distribution. The Gamma-Gamma distributed turbulence-induced irradiance fading I can be described by the PDF given by [31]

$$f_I(I) = \frac{2(pq)^{\left(\frac{p+q}{2}\right)}}{\Gamma(p)\Gamma(q)}I^{\left(\frac{p+q}{2}-1\right)}K_{p-q}\left(2\sqrt{pqI}\right), \tag{8}$$

where the parameters p and q represent the effective numbers of small-scale and large-scale cells of the scattering channel,

respectively, and are directly related to the scintillations of the transmitted optical beam [32]. $K_{p-q}(\cdot)$ is the modified Bessel function of the second kind. Assuming a Gaussian beam propagation, the parameters p and q are given by [31]

$$p = \frac{1}{\exp\left(\sigma^2_{\ln x}\right) - 1}$$
$$q = \frac{1}{\exp\left(\sigma^2_{\ln y}\right) - 1}, \tag{9}$$

where $\sigma^2_{\ln x}$ and $\sigma^2_{\ln y}$ are defined as the normalized variances of the received irradiance due to the scintillation caused by the large and small scale eddies in the turbulence channel. Under the assumption of the Kolmogorov power spectrum of atmospheric fluctuations, $\sigma^2_{\ln x}$ and $\sigma^2_{\ln y}$ are given by [31]

$$\sigma^2_{\ln x} = \frac{0.49\sigma_R^2}{\left[1 + 0.56\,(1+\Delta)\,\sigma_R^{12/5}\right]^{7/6}}$$
$$\sigma^2_{\ln y} = \frac{0.51\sigma_R^2}{\left[1 + 0.69\sigma_R^{12/5}\right]^{5/6}} \tag{10}$$

where σ_R^2 is defined in (5). $\Delta = [1+(\frac{2\,d_{TR}}{kW_0^2})^2]^{-1}$ represents the divergence in the optical beam while propagating a distance d_{TR}. W_0 is the initial beam radius.

The PDF distribution described in (8) is normalized with $\mathrm{E}[I] = 1$ with $\mathrm{E}[\cdot]$ representing the expectation operation. The NLOS UV link consists of two LOS paths, i.e., from the transmitter to the intersected volume and the other from the intersected volume to the receiver. For each path, we model the intensity fluctuations using Gamma-Gamma distribution and then combine the two individual paths to obtain the distribution of the NLOS path [13], [18]. The normalized PDF of the intensity fluctuations in the signal propagating from the transmitter to the intersected volume is given by

$$f_{I_v}(I_v) = \frac{2\,(p_v q_v)^{\left(\frac{p_v+q_v}{2}\right)}}{\Gamma(p_v)\,\Gamma(q_v)} I_v^{\left(\frac{p_v+q_v}{2}-1\right)} K_{p_v-q_v}\left(2\sqrt{p_v q_v I_v}\right), \tag{11}$$

where the parameters p_v and q_v can be evaluated using (9) with d_{TR} substituted by d_{tv}. With the scattered UV photons in the intersected volume acting as a new source towards the receiver, the conditional PDF of the intensity fluctuations at the receiver can then be given by

$$f_{I_r}(I_r\,|I_v) = \frac{2\,(p_r q_r)^{\left(\frac{p_r+q_r}{2}\right)}}{\Gamma(p_r)\,\Gamma(q_r)} I_r^{\left(\frac{p_r+q_r}{2}-1\right)} K_{p_r-q_r}\left(2\sqrt{p_r q_r I_r}\right), \tag{12}$$

The parameters p_r and q_r can readily be obtained using (9) with d_{TR} replaced by d_{vr}. The marginal PDF of the intensity fluctuations at the receiver is then given by

$$f_{I_r}(I_r) = \int_0^\infty f_{I_r}(I_r\,|I_v)\, f_{I_v}(I_v)\, dI_v, I_v > 0. \tag{13}$$

From (11), (12) and (13), and using the identities [33, eq. (14)] and [34, eq. (7.811.4)], the closed-form expression for the marginal PDF of I_r can be written as

$$f_{I_r}(I_r) = \frac{(p_v q_v)\,(p_r q_r)^{\left(\frac{p_r+q_r}{2}\right)}}{\Gamma(p_v)\,\Gamma(q_v)\,\Gamma(p_r)\,\Gamma(q_r)} I_r^{\left(\frac{p_r+q_r}{2}-1\right)} \times G^{2,0}_{0,2}\left[p_r q_r I_r \,\middle|\, \frac{p_r-q_r}{2}, -\frac{p_r-q_r}{2}\right], \tag{14}$$

where $G[\cdot]$ represents the Meijer G-function.

Remark 1: The instantaneously received signal $y(t)$, as illustrated in (1), is impaired by the multiplicative effect of the turbulence-induced fading I_r. Here, I_r is a random variable following the distribution given by (12). It is important to note that, the random variable I_r is normalized with statistical average $E[I_r] = 1$ and it includes the diffractive and refractive effects of the turbulence channel. The atmospheric scintillation represented by I_r is a slow time-varying process in optical communications [35].

B. VALIDATION OF THE TURBULENCE MODEL

We point out that the marginal PDF, as illustrated in (14), is based on the fact that each scattered path is Gamma-Gamma distributed. The Gamma-Gamma model is based on the modulation process where the scintillation effect is assumed to consist of small-scale and large-scale irradiance fluctuations. The small-scale fluctuations are contributed by the eddies smaller than the Fresnel zone or the coherence radius, whereas the large-scale fluctuations are contributed by the cells greater than the Fresnel zone [24].

It is well documented that, unlike the log-normal distribution that is based on the Rytov approximation and is valid only in weak turbulence regime over shorter propagation links, the Gamma-Gamma distribution is valid over all turbulence regimes, that is, from weak to strong turbulence, and shows a remarkably good fit with experimental data [23], [36]. Therefore, based on the fact that each scattered path is Gamma-Gamma distributed, it is valid that the PDF model obtained in (14) is applicable across all conditions of atmospheric turbulence.

C. STATISTICAL ANALYSIS: CDF OF THE LARGEST ORDER STATISTICS

The CDF of I_r, defined as $F_{I_r}(I_r) = \int_0^{I_r} f_{I_r}(I_r)dI_r$, is derived using the identity [37, eq. (07.34.21.0084.01)] as shown

$$F_{I_r}(I_r) = \frac{(p_v q_v)\,(p_r q_r)^{\left(\frac{p_r+q_r}{2}\right)}}{\Gamma(p_v)\,\Gamma(q_v)\,\Gamma(p_r)\,\Gamma(q_r)} I_r^{\left(\frac{p_r+q_r}{2}\right)} \times G^{2,1}_{1,3}\left[p_r q_r I_r \,\middle|\, \frac{p_r-q_r}{2}, -\frac{\frac{2-p_r-q_r}{2}}{\frac{p_r}{2}\,q_r}, -\frac{p_r+q_r}{2}\right]. \tag{15}$$

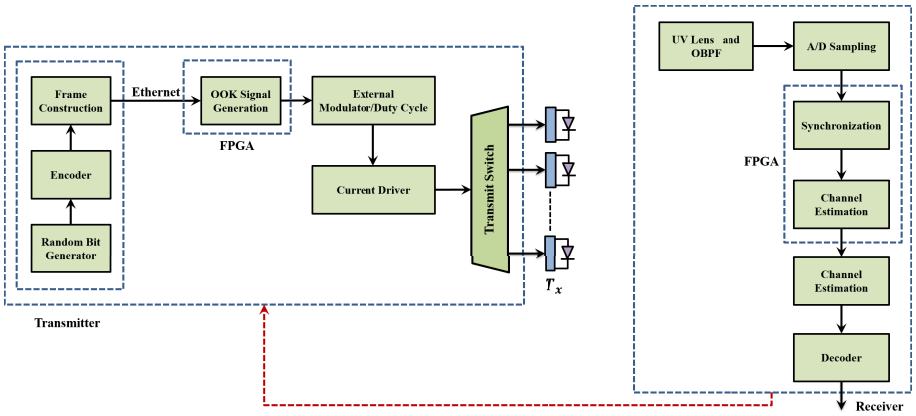

FIGURE 3. Realization of the transceiver section.

Assuming the channel irradiance to be an independent and identically distributed random variable, the CDF of the largest order statistics $I_{r,\max}$ can then be formulated as

$$\begin{aligned} F_{I_{r,\max}}\left(I_{r,\max}\right) &= P_r\left[I_{r,\max} \leq I_r\right] \\ &= P_r\left[\underset{\forall j=1,2,\ldots,L}{I_{r,j}} \leq I_r\right] \\ &= \left[F_{I_r}\left(I_r\right)\right]^L. \end{aligned} \tag{16}$$

Using (16), the PDF of the largest order statistics can then be obtained as $f_{I_{r,\max}}\left(I_{r,\max}\right) = L\left[F_{I_r}\left(I_r\right)\right]^{L-1} f_{I_r}\left(I_r\right)$. Considering the transmit diversity with two branches, i.e., $L = 2$, the closed-form expression for the PDF of the largest order statistics is obtained as shown in (17), as shown at the bottom of the next page.

We like to point out that, for brevity, we assume that all the transmitters are located at sufficient distances from each other. Following this assumption, we consider that the transmitter signals are uncorrelated in obtaining (17).

III. SYSTEM DESIGN AND PERFORMANCE ANALYSIS

In this section, we present transceiver design and derive the expressions for the average bit error rate, the outage probability, and the channel capacity.

A. REALIZATION OF THE TRANSMITTER AND RECEIVER SECTIONS

The goal of this subsection is to provide a simple prototype for the realization of the transmitter and the receiver section and to implement the proposed system. The transceiver section is illustrated in Fig. 3 and consists of a random bit generator and an encoder. The output of the encoder is divided into the transmission frames and is applied at the input of the FPGA board. The FPGA board can be used to feed the binary sequence to the driver circuit that powered the transmitter section. The synchronization and pilot bits are added at the head of each frame which is then used to drive the UV laser/LED driver circuit. To transmit the optical signal in the UV-C band, a UVTOP280 LED can be considered with a nominal peak wavelength of 280 nm, which delivers typically 1.3 mW power at the forward current of 20 mA.

At the receiver, the incoming petahertz signal is passed through a lens followed by an optical bandpass filter (OBPF), as illustrated in Fig. 3. OBPF is utilized to minimize the amount of background radiation noise at the input of the photodetector. We consider Gallium Nitride (GaN) photodetector to measure the petahertz signal at the receiver. The photodetector converts the optical radiation into an electrical signal and is followed by a sampler and a threshold detector. At the receiver side, synchronous detection to limit low-frequency temporal clutter terrestrial illumination sources is considered that enables a well-defined narrow temporal passband. A solar-blind window is placed in front of the photodetector. There may be a spectral mismatch between the transmitter and the filter and should be taken care of [38]–[40].

We like to point out that, for brevity, the amplification at the receiver is ignored in this work. That, in turn, enables to safely ignore the amplified spontaneous-emission noise [41] at the receiver. Moreover, since there is no amplification of the received power, the gain saturation by amplified spontaneous-emission noise can be neglected, which is typically the case at the receiver with low amplification gain [42], [43].

Remark 2: It is important to note that, in optical communications, the time scales of the atmospheric turbulence fading are far larger than the bit duration and therefore, this block fading channel is often termed as a slow fading optical channel [25], [44]. Therefore, as described in [45], and as depicted in Fig. 2, the knowledge of the channel condition at the transmitter side is possible in optical turbulence channel as the turbulence fading is a slow fading process.

Considering $L = 2$, in order to validate the system, we derive important performance metrics including average bit error rate, outage probability, and the channel capacity.

It should be noted that using similar procedures the expressions for the performance metrics can also be obtained for higher L values.

B. AVERAGE BIT ERROR RATE

In optical wireless communications, the instantaneous SNR is proportional to the square of the average received optical signal power, rather proportional to the received power. Therefore, utilizing (1), the instantaneous received electrical SNR at the receiver can be modeled as

$$\chi = \frac{(SHP_t)^2 I_{r,\max}^2}{N_0}. \tag{18}$$

As defined in [46], the average electrical SNR can be written as

$$^1\xi = \frac{\left(SHP_t E[I_{r,\max}]\right)^2}{N_0} = \frac{(SHP_t)^2}{N_0}. \tag{19}$$

Remark 3: It is to be noted that we assume a fixed total transmit power budget P_{Total}, such that the average transmit optical power assigned to each branch is given by $P_t = P_{Total}/L$, where P_{Total} is constant and is independent of the number of diversity branches L.

The conditional BER for non-return-to-zero OOK modulated signal can then be written as $P_e\left(\chi \left| I_{r,\max}\right.\right) = \frac{1}{2}\text{erfc}\left(\frac{1}{2\sqrt{2}}\sqrt{\xi I_{r,\max}^2}\right)$, where erfc$(\cdot)$ represents the complementary error function [47]. The average BER P_e can be obtained by averaging $P_e\left(\chi \left| I_{r,\max}\right.\right)$ over the distribution of $I_{r,\max}$

$$P_e = \int_0^\infty P_e\left(\chi \left| I_{r,\max}\right.\right) f_{I_{r,\max}}\left(I_{r,\max}\right) dI_{r,\max}. \tag{20}$$

Substituting for $f_{I_{r,\max}}\left(I_{r,\max}\right)$ from (17) into (20) and using the identity [37, eq. 07.34.03.1081.01]

$$G_{0,m}^{m,0}\left[z \left| b, b+\frac{1}{m}, b+\frac{\overline{2}}{m}, \cdots, b+\frac{m-1}{m}\right.\right] = \frac{(2\pi)^{\frac{m-1}{2}}}{\sqrt{m}} z^b \exp\left(-mz^{\frac{1}{m}}\right), \tag{21}$$

(20) can be rewritten as shown in (22), as shown at the bottom of the next page.

The product of the two Meijer G-functions in (22) can then readily be solved using the identity [48, eq. (1)], that yields (23), as shown at the bottom of the next page. $\mathbf{S}[\cdot]$ in (23) is the extended generalized bivariate as defined in [49]. Equation (23) represents the average BER in integral form. The integral in (23) can be solved to a closed-form expression by using the identity [49, eq. (2.1)] as derived in (24), as shown at the bottom of the next page.

C. OUTAGE PROBABILITY

In this section, we consider another important performance criterion characteristic, that is, the outage probability, of the proposed system operating over the Gamma-Gamma distributed fading channel. The outage probability $P_{out}(\chi_{Th})$ is defined as the probability that the instantaneously received SNR χ falls below a certain predetermined threshold χ_{Th}. Mathematically, the outage probability is defined as [50]

$$P_{out}(\chi_{Th}) = P_r\left[\chi < \chi_{Th}\right] = \int_0^{\chi_{Th}} f_\chi(\chi) d\chi, \tag{25}$$

where $f_\chi(\chi)$ represents the distribution of the instantaneously received SNR χ. Applying the Jacobean transformation, $f_\chi(\chi)$ is derived as illustrated in (26), as shown at the bottom of page 9.

Substituting (26) into (25) and utilizing the identity [33, eq. (14)] with some simple mathematical operations, the outage probability in integral from can be represented as depicted in (27), as shown at the bottom of page 9, where the operator $\lfloor\cdot\rfloor$ in (27) denotes the ceiling operation.

The integral part in (27) can readily be solved by using the identity [37, eq. (07.34.21.0084.01)] that yields the expression for the outage probability as illustrated in (28), as shown at the bottom of page 9.

D. OPTICAL CHANNEL CAPACITY

Assuming perfect channel state information at the transmitter with no power adaptation, the average optical channel capacity of the proposed system can be defined as [6]

$$C_{avg} = \int_0^\infty \log_2\left(1+\xi I_{r,\max}^2\right) f_{I_{r,\max}}\left(I_{r,\max}\right) dI_{r,\max} \tag{29}$$

Substituting (17) into (29) and using the identities [33, eq. (11)] and [37, eq. (07.34.03.0404.01)], the modified

$$f_{I_{r,\max}}\left(I_{r,\max}\right) = \frac{2\left[\left(p_v q_v\right)\left(p_r q_r\right)^{\left(\frac{p_r+q_r}{2}\right)}\right]^2}{\left[\Gamma\left(p_v\right)\Gamma\left(q_v\right)\Gamma\left(p_r\right)\Gamma\left(q_r\right)\right]^2} I_{r,\max}^{(p_r+q_r-1)} \times G_{0,2}^{2,0}\left[p_r q_r I_{r,\max}\left| \frac{p_r-q_r}{2}, \overline{-\frac{p_r-q_r}{2}}\right.\right] G_{1,3}^{2,1}\left[p_r q_r I_{r,\max}\left| \frac{p_r-q_r}{2}, \frac{\frac{2-p_r-q_r}{2}}{-\frac{p_r}{2}q_r}, -\frac{p_r+q_r}{2}\right.\right]. \tag{17}$$

expression for the average channel capacity can be written as shown in (30), as shown at the bottom of page 10.

The integration in (30) can be solved using the identity [33, eq. (21)] and can be derived as shown in (31), as shown at the bottom of page 10.

$$P_e(\xi) = -\frac{(p_v q_v)^2 (p_r q_r)^{\left(\frac{3p_r+q_r}{2}\right)}}{4\pi \left[\Gamma(p_v)\Gamma(q_v)\Gamma(p_r)\Gamma(q_r)\right]^2} \int_0^{\infty} I_{r,\max}^{\left(\frac{3p_r+q_r-2}{2}\right)} \exp\left(-2\sqrt{p_r q_r I_{r,\max}}\right) \times G_{2,6}^{4,2}\left[\frac{(p_r q_r)^2 I_{r,\max}^2}{16}\middle| \begin{matrix} \frac{p_r-q_r}{4}, \frac{p_r-q_r+2}{4} \\ \frac{2-p_r-q_r}{4}, \frac{4-p_r-q_r}{4}, \frac{q_r-p_r}{4}, \frac{q_r-p_r+2}{4}, \frac{-p_r-q_r}{4}, \frac{2-p_r-q_r}{4} \end{matrix}\right] \times G_{1,2}^{2,0}\left[\frac{\xi I_{r,\max}^2}{8}\middle| \begin{matrix} 1 \\ 0, \frac{1}{2} \end{matrix}\right] dI_{r,\max}. \tag{22}$$

$$P_e(\xi) = -\frac{(p_v q_v)^2 (p_r q_r)^{\left(\frac{3p_r+q_r}{2}\right)}}{4\pi \left[\Gamma(p_v)\Gamma(q_v)\Gamma(p_r)\Gamma(q_r)\right]^2} \int_0^{\infty} I_{r,\max}^{\left(\frac{3p_r+q_r-2}{2}\right)} \exp\left(-2\sqrt{p_r q_r I_{r,\max}}\right) \times \mathbf{S}\left[\begin{matrix} \begin{bmatrix} 0,0 \\ 0,0 \end{bmatrix} \\ \begin{pmatrix} 2,4 \\ 0,2 \end{pmatrix} \\ \begin{pmatrix} 0,2 \\ 1,0 \end{pmatrix} \end{matrix}\middle| \begin{matrix} \frac{2-p_r-q_r}{4}, \frac{4-p_r-q_r}{4}; \frac{p_r-q_r}{4}, \frac{p_r-q_r+2}{4}, \frac{q_r-p_r}{4}, \frac{q_r-p_r+2}{4}, \frac{-p_r-q_r}{4}, \frac{2-p_r-q_r}{4} \\ 1; 0, 2 \end{matrix}; -\right] \begin{matrix} \frac{(p_r q_r I_{r,\max})^2}{16} \\ \frac{\xi I_{r,\max}^2}{8} \end{matrix} \Bigg] dI_{r,\max}. \tag{23}$$

$$P_e(\xi) = \frac{2^{\left(\frac{6p_r+2q_r-7}{2}\right)} (p_v q_v)^2 (p_r q_r)^{-q_r}}{\pi^{\frac{5}{2}} \left[\Gamma(p_v)\Gamma(q_v)\Gamma(p_r)\Gamma(q_r)\right]^2} \times S\left[\begin{matrix} \begin{bmatrix} 4,0 \\ 0,0 \end{bmatrix} \\ \begin{pmatrix} 2,4 \\ 0,2 \end{pmatrix} \\ \begin{pmatrix} 0,2 \\ 1,0 \end{pmatrix} \end{matrix}\middle| \begin{matrix} \frac{3p_r+q_r}{4}, \frac{3p_r+q_r+1}{4}, \frac{3p_r+q_r+2}{4}, \frac{3p_r+q_r+3}{4}; - \\ \frac{2-p_r-q_r}{4}, \frac{4-p_r-q_r}{4}; \frac{p_r-q_r}{4}, \frac{p_r-q_r+2}{4}, \frac{q_r-p_r}{4}, \frac{q_r-p_r+2}{4}, \frac{-p_r-q_r}{4}, \frac{2-p_r-q_r}{4} \\ 1; 0, 2 \end{matrix}\right] \begin{matrix} 1 \\ \frac{2\xi}{(p_r q_r)^2} \end{matrix} \Bigg]. \tag{24}$$

IV. RESULTS AND DISCUSSIONS

A. SIMULATION SETUP AND METHODOLOGY

To obtain good statistical averages, we generate 10^5 realizations of the random variable I_r for each set of parameters $\{p_v, q_v, p_r, q_r\}$. All the results are computed using MATLAB (R2018b) software [51]. The Meijer G-function is a built-in routine in prevalent computing software such as MATLAB, MAPLE, and MATHEMATICA, the bivariate Meijer G-function is available in MATHEMATICA [52]. In addition, a fast MATLAB algorithm with automated integration contour for the generalized bivariate Meijer G-function can be found in [53]. To realize the random variable I_r theoretically for a given turbulence strength (for a particular C_n^2 value), we first calculate σ_R^2 using (4). Utilizing σ_R^2, the values of $\sigma_{\ln x}^2$ and $\sigma_{\ln y}^2$ are evaluated using (10). $\{p_v, q_v, p_r, q_r\}$ are then obtained using (9). These values are then used to realize $I_{r,\max}$ using (17). The total noise variance of the random noise is set to 0.25.

Unless otherwise specified, the total transmit power budget P_{Total} is set to 20 dBm. The other parameters considered in performance evaluation are listed in Table 1. Moreover,

$$f_\chi(\chi) = \frac{\left[(p_v q_v)\,(p_r q_r)^{\left(\frac{p_r+q_r}{2}\right)}\right]^2}{[\Gamma(p_v)\,\Gamma(q_v)\,\Gamma(p_r)\,\Gamma(q_r)]^2}\left(\frac{1}{\xi}\right)^{\left(\frac{p_r+q_r}{2}\right)} \times \chi^{\left(\frac{p_r+q_r}{2}-1\right)} G_{0,2}^{2,0}\left[p_r q_r\sqrt{\frac{\chi}{\xi}}\,\middle|\,\frac{p_r-q_r}{2}, -\frac{p_r-q_r}{2}\right] G_{1,3}^{2,1}\left[p_r q_r\sqrt{\frac{\chi}{\xi}}\,\middle|\,\frac{p_r-q_r}{2}, \frac{2-p_r-q_r}{2}, -\frac{p_r+q_r}{2}\right]. \quad (26)$$

$$P_{out}(\chi_{Th}) = \frac{\left[(p_v q_v)\,(p_r q_r)^{\left(\frac{p_r+q_r}{2}\right)}\right]^2}{[\Gamma(p_v)\,\Gamma(q_v)\,\Gamma(p_r)\,\Gamma(q_r)]^2}\left(\frac{1}{\xi}\right)^{\left(\frac{p_r+q_r}{2}\right)} \times\sqrt{2\pi}\sum_{k=0}^{\infty}\left\{\frac{(-1)^k}{k!}\sum_{j=0}^{\lfloor |p_r-q_r|-\frac{1}{2}\rfloor}\left[\frac{\left(j+|p_r-q_r|-\frac{1}{2}\right)!}{j!\left(-j+|p_r-q_r|-\frac{1}{2}\right)!}2^{k-2j-\frac{1}{2}}(p_r q_r)^{\left(\frac{2k-2j-1}{4}\right)}\left(\frac{1}{\xi}\right)^{\left(\frac{2k-2j-1}{8}\right)}\right.\right. \times\int_0^{\chi_{Th}}\chi^{\left(\frac{4p_r+4q_r+2k-2j-1}{8}-1\right)} G_{1,3}^{2,1}\left[p_r q_r\sqrt{\frac{\chi}{\xi}}\,\middle|\,\frac{p_r-q_r}{2}, \frac{2-p_r-q_r}{2}, -\frac{p_r+q_r}{2}\right] d\chi\left.\right]\right\}. \quad (27)$$

$$\begin{aligned} P_{out}(\chi_{Th}) &= \frac{\left[(p_v q_v)\,(p_r q_r)^{\left(\frac{p_r+q_r}{2}\right)}\right]^2}{\sqrt{8\pi}\,[\Gamma(p_v)\,\Gamma(q_v)\,\Gamma(p_r)\,\Gamma(q_r)]^2}\left(\frac{1}{\xi}\right)^{\left(\frac{p_r+q_r}{2}\right)} \times\sqrt{2\pi}\sum_{k=0}^{\infty}\left\{\frac{(-1)^k}{k!}\sum_{j=0}^{\lfloor |p_r-q_r|-\frac{1}{2}\rfloor}\left[\frac{\left(j+|p_r-q_r|-\frac{1}{2}\right)!}{j!\left(-j+|p_r-q_r|-\frac{1}{2}\right)!}2^{k-2j-\frac{1}{2}}(p_r q_r)^{\left(\frac{2k-2j-1}{4}\right)}\left(\frac{1}{\xi}\right)^{\left(\frac{2k-2j-1}{8}\right)}\right.\right. \\ &\times\chi_{Th}^{\left(\frac{4p_r+4q_r+2k-2j-1}{8}\right)} \times G_{3,7}^{4,3}\left[\left(\frac{2p_r q_r}{\sqrt{\xi}}\right)^2\chi_{Th}^4\right. \\ &\left.\left.\left.\left|\frac{p_r-q_r}{4}, \frac{p_r-q_r+2}{4}, \frac{9-4p_r-4q_r-2k+2j}{8}, \frac{2-p_r-q_r}{4}, \frac{4-p_r-q_r}{4}\right.\right.\right.\right. \\ &\left.\left.\left.\left.\frac{q_r-p_r}{4}, \frac{q_r-p_r+2}{4}, -\frac{p_r+q_r}{4}, -\frac{p_r+q_r-2}{4}, \frac{1-4p_r-4q_r-2k+2j}{8}\right]\right]\right\}. \end{aligned} \quad (28)$$

TABLE 1. System parameters.

Parameter	Value
Optical frequency	1.07 Petahertz
Modulation bandwidth	20 MHz
Rayleigh scattering coefficient [54]	0.49 km^{-1}
Extinction coefficient [54]	0.74 km^{-1}
Scattering phase function q_s	1 (Isotropic scattering)
$\{\psi_t, \psi_r, \phi_t, \phi_r\}$	$\{\pi/4, \pi/4, \pi/180, \pi/3\}$
Outage threshold χ_{Th}	5 dB

TABLE 2. GaN photodetector specifications [55].

GaN specifications	Value
Sensitivity	200 − 365 nm
Active detector area (mm^2)	6.25
Quantum efficiency (%)	29 A/W
Dark current (equivalent photon flux) ($ph/cm^2/\mu s$)	10^7
Rise/fall time (μs)	10
Packaging	TO-5 can

the specifications of the GaN photodetector are provided in TABLE 2.

We like to point to that the infinite sum in Eqs. (28) and (31) converges for any value of the parameters p_v, q_v, p_r, q_r. However, for (28), more than 52 terms are needed for summation to achieve accuracy at the 5th significant digit. Whereas for (31), to achieve accuracy at the 5th significant digit, more than 24 terms are required.

Remark 4: It should be noted that, for all the results, the average SNR is evaluated in the electrical domain.

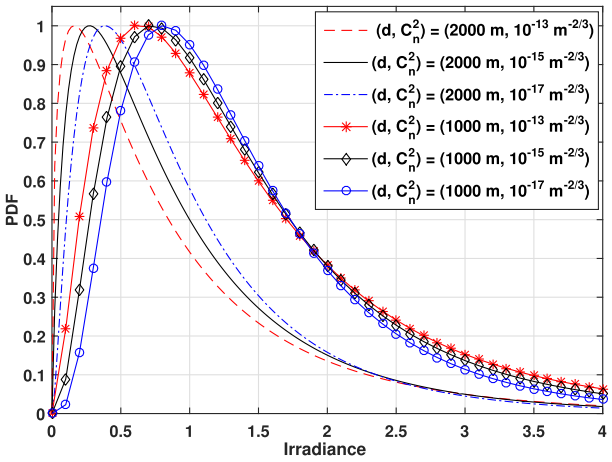

FIGURE 4. PDF of the atmospheric scintillation for the NLOS links over different turbulence fading strengths and baseline distances.

B. RESULTS ANALYSIS

The PDF of the received irradiance over the NLOS scattered link for different turbulence strengths and baseline distances is illustrated in Fig. 4. It can be observed that, on increasing the baseline distance or the refractive index structure parameter C_n^2, the effect of the turbulence increases, and the peak of the PDF profile shifts towards the left. This can be attributed to the fact that with increasing baseline distance d or C_n^2, the beam propagation effect is weakened by the loss of spatial coherence. Under weak turbulence condition with $C_n^2 = 10^{-17}$ $m^{-2/3}$, the Fresnel zone size defines the dominant scale size for the irradiance fluctuation. Under weak turbulence regimes, the Fresnel zone is smaller than the transverse coherence spatial radius. However, as the refractive index structure parameter increases to a higher value, say,

$$C_{avg} = \frac{\ln(4)\left[(p_v q_v)\,(p_r q_r)^{\left(\frac{p_r+q_r}{2}\right)}\right]^2}{[\Gamma(p_v)\,\Gamma(q_v)\,\Gamma(p_r)\,\Gamma(q_r)]^2} \times \sum_{k=0}^{\infty} \frac{(-1)^k\,\xi^{k+1}}{k!\Gamma(k+2)} \int_0^{\infty} I_{r,\max}^{(2k+p_r+q_r-1)} G_{0,2}^{2,0}\left[p_r q_r I_{r,\max} \middle| \frac{p_r-q_r}{2}, \frac{q_r-p_r}{2}\right] \times G_{1,3}^{2,1}\left[p_r q_r I_{r,\max} \middle| \frac{p_r-q_r}{2}, \frac{\frac{2-p_r-q_r}{2}}{\frac{q_r-p_r}{2}}, -\frac{p_r+q_r}{2}\right] dI_{r,\max}. \tag{30}$$

$$C_{avg} = \frac{\ln(4)\left[(p_v q_v)\,(p_r q_r)^{\left(\frac{p_r+q_r}{2}\right)}\right]^2}{[\Gamma(p_v)\,\Gamma(q_v)\,\Gamma(p_r)\,\Gamma(q_r)]^2} \times \sum_{k=0}^{\infty} \frac{(-1)^k\,\xi^{k+1}}{k!\Gamma(k+2)} (p_r q_r)^{-(2k+p_r+q_r)} G_{3,3}^{2,3}\left[1 \middle| \frac{2-p_r-q_r}{2}, \frac{2-4k-3p_r-q_r}{2}, \frac{2-4k-p_r-3q_r}{2} \atop \frac{p_r-q_r}{2}, d\frac{q_r-p_r}{2}, -\frac{p_r+q_r}{2}\right]. \tag{31}$$

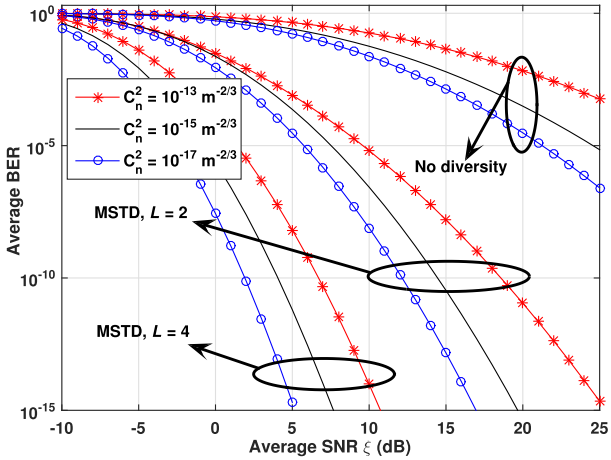

FIGURE 5. Bit error rate performance against the average received SNR over different turbulence channels.

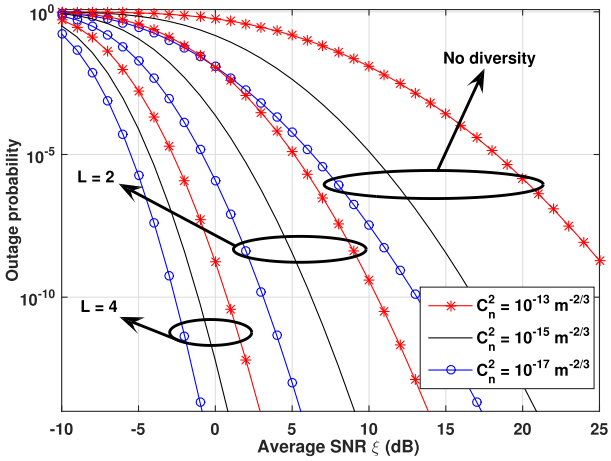

FIGURE 6. Outage probability against the average received SNR over the turbulence channel.

$C_n^2 = 10^{-13}$ m$^{-2/3}$, the Fresnel zone becomes larger than the coherence spatial radius, and therefore the optical channel impairment due to the turbulence increases.

From the expression obtained in (24), the average bit error rate performance of the proposed system can be determined for any given value of the average SNR. To illustrate this, simulation results of the average bit error rate against the average SNR are shown in Fig. 5. We consider two cases, that is, $L = 2$ and $L = 4$ with all the transmitters oriented in the same direction towards the receiver. Moreover, for comparison, a transmit scenario with no diversity ($L = 1$) is also considered. The following conclusions can be drawn from the results. As expected, a higher level of degradation in the BER performance due to the atmospheric turbulence occurs in the transmitting scenario with no diversity. As can be seen, at an average received SNR of 25 dB and $C_n^2 = 10^{-13}$ m$^{-2/3}$, the BER performance for no diversity scenario improves significantly from 10^{-3} to 5×10^{-15} when the proposed system is applied with $L = 2$. Moreover, the proposed system is found to boost the BER performance significantly under low SNR regimes when compared with the case where no spatial diversity is employed. As illustrated, at a low received SNR value of 5 dB and $C_n^2 = 10^{-17}$ m$^{-2/3}$, the BER attains a value of approximately 5×10^{-15} with $L = 4$. The results obtained demonstrate a significant improvement in the performance as the number of diversity branches L increases. From the results, it can be concluded that the proposed scheme is useful in applications where there is a power constraint or increasing the power requirement in the link budget is impractical to overcome the turbulence-induced fading.

Figure 6 shows a comparative analysis of the outage probability of the NLOS UV communication system under different turbulence regime with different diversity branches. As a reference performance, the outage probability of the NLOS UV system without diversity is also presented. It can be seen that the performance of the system is highly dependent on the L value and as expected, the UV system with a higher L value

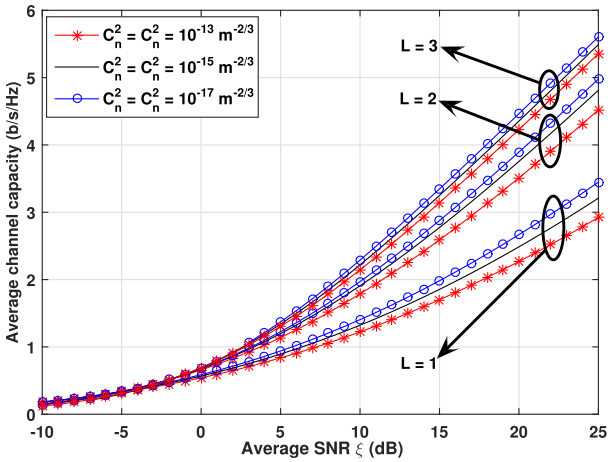

FIGURE 7. Average channel capacity against the average received SNR over the turbulence channel.

has the best performance. Furthermore, it can also be seen that under the strong atmospheric turbulence condition, when the number of diversity branches is increased from $L = 1$ to $L = 2$ and $L = 4$, the required average electrical SNR is reduced by 13 dB and 21 dB, respectively, for the outage probability of 10^{-5}.

The optical channel capacity per unit bandwidth with perfect channel state information at the transmitter is illustrated in Fig. 7. As can be noticed from these results, the use of the transmit diversity helps in achieving higher capacity. However, it is interesting to note that with no power adaptation at the transmitter, as the number of branches increases, the curves under different turbulence regimes come closer.

Figure 8 illustrates the average bit error rate against the baseline distance under different turbulence regimes. With the transmit power set to 20 dBm, the performance degrades as the baseline distance increases. This can be attributed to the fact that, as the baseline distance increases, the atmospheric attenuation and absorption increase. As illustrated, for $d = 200$ m and C_n^2 set to 10^{-17} m$^{-2/3}$, the achievable BER is

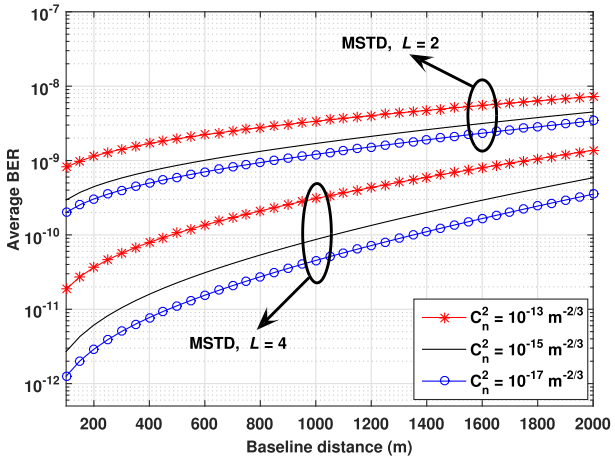

FIGURE 8. Bit error rate performance against the baseline distance over different turbulence strengths ($P_{Total} = 20$ dBm).

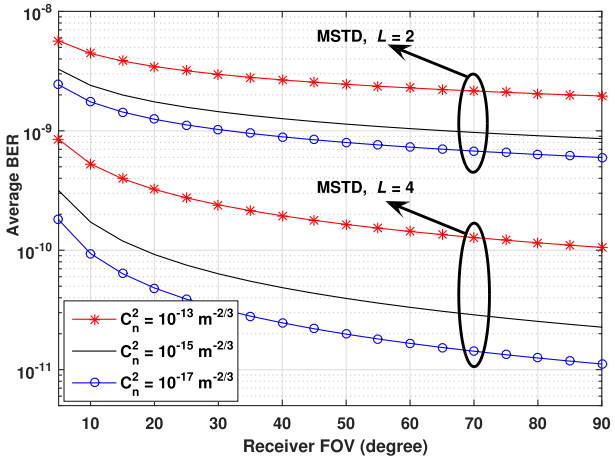

FIGURE 9. Bit error rate performance relative to the receiver FOV over different turbulence channels ($P_{Total} = 20$ dBm).

3×10^{-12} and 2×10^{-10} for $L = 4$ and 2, respectively. As depicted, on increasing the distance to 2000 m, the BER increases to 3.5×10^{-10} and 1.5×10^{-9} for $L = 4$ and 2, respectively. However, it is interesting to note that, for all the turbulence regimes with a longer baseline distance of up to 2000 m, the achievable BER in the proposed system is always less than the maximum acceptable threshold value of 10^{-6}. Therefore, these results justify the adoption of the proposed transmit diversity scheme for the NLOS UV link because it is impractical for many optical applications to increase the transmit power constraint in the link budget to eliminate the path loss observed over a longer propagation path.

To analyze the performance dependence of the proposed system on the parameters of UV link geometry, the average bit error rate against the receiver FOV is presented in Fig. 9. The performance is found to be very sensitive to the receiver FOV. This can be attributed to the fact that a larger FOV value results in more received optical power, thereby resulting in a high received SNR value.

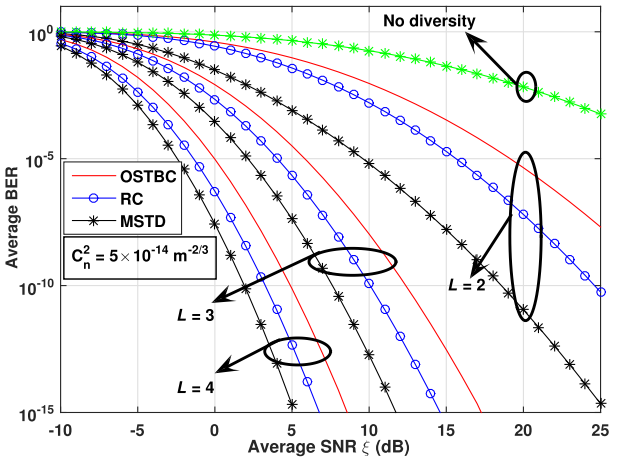

FIGURE 10. BER performance comparison of the MSTD technique with RC and OSTBC in the optical scattering communication link over the turbulence channel.

In Fig. 10, it is shown that the proposed maximal selective transmit diversity technique (MSTD) based on the selection of the optical path with a greater value of irradiance extracts full diversity and provides better performance, compared to RC and OSTBC. As illustrated, for instance, at an average SNR of 20 dB with C_n^2 set to 5×10^{-14} m$^{-2/3}$, the average BER for $L = 2$ is approximately equal to 5×10^{-6} for OSTBC and 10^{-7} for RC, whereas, for the proposed MSTD, it is found to be 10^{-11}. Moreover, it is important to note that, the performance difference between the MSTD and the RC decreases gradually with increasing L. For instance, to maintain a target BER of 1×10^{-10}, the average SNR required for MSTD and RC for $L = 2$ is 18 dB and 25 dB, respectively. However, when $L = 4$, the average SNR required for MSTD and RC is 3 dB and 4 dB, respectively.

V. CONCLUSION

The design and analysis of the maximal selective transmit diversity for NLOS optical petahertz communications have been proposed, utilizing the continuous waveform detector over the optical channel corrupted by atmospheric turbulence. Knowing the fact that turbulence fading is a slow time-varying process, we assumed that the information about the channel conditions are available at the transmitter. We have characterized the received signal by a continuous waveform with each scattered path experiencing the Gamma-Gamma distributed turbulence fading. The CDF of the largest order statistics of the received irradiance has been quantified and subsequently the closed-form analytical expression for the average bit error rate has been derived. Furthermore, the analytical expressions for the outage probability and the average optical channel capacity have been evaluated. From these derived expressions, we have presented a comprehensive performance analysis of the proposed system. It is demonstrated that at low received SNR value of 5 dB and at a turbulence strength of $C_n^2 = 10^{-17}$ m$^{-2/3}$, the BER performance of the proposed technique attains a value of approximately

5×10^{-15} with $L = 4$. It is shown that the maximal selection transmit diversity significantly outperforms the RC and OSTBC techniques. The results obtained justify the proposed maximal selective transmit diversity scheme over severe turbulence fading in petahertz optical wireless communications.

REFERENCES

[1] E. E. Elsayed and B. B. Yousif, "Performance enhancement of M-ary pulse-position modulation for a wavelength division multiplexing free-space optical systems impaired by interchannel crosstalk, pointing error, and ASE noise," *Opt. Commun.*, vol. 475, Nov. 2020, Art. no. 126219.

[2] B. B. Yousif and E. E. Elsayed, "Performance enhancement of an orbital-angular-momentum-multiplexed free-space optical link under atmospheric turbulence effects using spatial-mode multiplexing and hybrid diversity based on adaptive MIMO equalization," *IEEE Access*, vol. 7, pp. 84401–84412, 2019.

[3] M. Singh and J. Malhotra, "Long-reach high-capacity hybrid MDM-OFDM-FSO transmission link under the effect of atmospheric turbulence," *Wireless Pers. Commun.*, vol. 107, no. 4, pp. 1549–1571, Aug. 2019.

[4] P. Saxena and M. R. Bhatnagar, "1-bit feedback-based beamforming scheme for an uplink FSO-NOMA system with SIC errors," *Appl. Opt.*, vol. 59, no. 36, pp. 11274–11291, Dec. 2020.

[5] Z. Xu and B. M. Sadler, "Ultraviolet communications: Potential and state-of-the-art," *IEEE Commun. Mag.*, vol. 46, no. 5, pp. 67–73, May 2008.

[6] S. Arya and Y.-H. Chung, "Multiuser interference-limited petahertz wireless communications over Málaga fading channels," *IEEE Access*, vol. 8, pp. 137356–137369, 2020.

[7] S. Arya and Y. H. Chung, "Novel indoor ultraviolet wireless communication: Design implementation, channel modeling, and challenges," *IEEE Syst. J.*, vol. 15, no. 2, pp. 2349–2360, Jun. 2021.

[8] M. Noshad, M. Brandt-Pearce, and S. G. Wilson, "NLOS UV communications using M-ary spectral-amplitude-coding," *IEEE Trans. Commun.*, vol. 61, no. 4, pp. 1544–1553, Apr. 2013.

[9] S. Arya and Y. H. Chung, "Non-line-of-sight ultraviolet communication with receiver diversity in atmospheric turbulence," *IEEE Photon. Technol. Lett.*, vol. 30, no. 10, pp. 895–898, May 15, 2018.

[10] S. Arya and Y. Ho Chung, "Spectrum sensing for optical wireless scattering communications over Málaga fading—A cooperative approach with hard decision fusion," *IEEE Trans. Commun.*, vol. 69, no. 7, pp. 4615–4631, Jul. 2021.

[11] M. R. Luettgen, J. H. Shapiro, and D. M. Reilly, "Non-line-of-sight single-scatter propagation model," *J. Opt. Soc. Amer. A, Opt. Image Sci.*, vol. 8, no. 12, pp. 1964–1972, 1991.

[12] H. Yin, S. Chang, X. Wang, J. Yang, J. Yang, and J. Tan, "Analytical model of non-line-of-sight single-scatter propagation," *J. Opt. Soc. Amer.*, vol. 27, no. 7, pp. 1505–1509, 2010.

[13] H. Ding, G. Chen, A. K. Majumdar, B. M. Sadler, and Z. Xu, "Turbulence modeling for non-line-of-sight ultraviolet scattering channels," *Proc. SPIE*, vol. 8038, May 2011, Art. no. 80380J.

[14] H. Ding, G. Chen, A. K. Majumdar, B. M. Sadler, and Z. Xu, "Modeling of non-line-of-sight ultraviolet scattering channels for communication," *IEEE J. Sel. Areas Commun.*, vol. 27, no. 9, pp. 1535–1544, Dec. 2009.

[15] C. Gong and Z. Xu, "Non-line of sight optical wireless relaying with the photon counting receiver: A count-and-forward protocol," *IEEE Trans. Wireless Commun.*, vol. 14, no. 1, pp. 376–388, Jan. 2015.

[16] M. H. Ardakani and M. Uysal, "Relay-assisted OFDM for NLOS ultraviolet communication," in *Proc. 17th Int. Conf. Transparent Opt. Netw. (ICTON)*, Jul. 2015, pp. 1–4.

[17] S. Arya and Y. H. Chung, "Amplify-and-forward multihop non-line-of-sight ultraviolet communication in the gamma–gamma fading channel," *J. Opt. Commun. Netw.*, vol. 11, no. 8, pp. 422–436, 2019.

[18] M. H. Ardakani, A. R. Heidarpour, and M. Uysal, "Performance analysis of relay-assisted NLOS ultraviolet communications over turbulence channels," *J. Opt. Commun. Netw.*, vol. 9, no. 1, pp. 109–118, 2017.

[19] A. Refaai, M. Abaza, M. S. El-Mahallawy, and M. H. Aly, "Performance analysis of multiple NLOS UV communication cooperative relays over turbulent channels," *Opt. Exp.*, vol. 26, no. 16, pp. 19972–19985, 2018.

[20] M. H. Ardakani, A. R. Heidarpour, and M. Uysal, "Performance analysis of MIMO NLOS UV communications over atmospheric turbulence channels," in *Proc. IEEE Wireless Commun. Netw. Conf.*, Apr. 2016, pp. 1–5.

[21] M. H. Ardakani, A. R. Heidarpour, and M. Uysal, "Non-line-of-sight ultraviolet communications over atmospheric turbulence channels," in *Proc. 4th Int. Workshop Opt. Wireless Commun. (IWOW)*, Sep. 2015, pp. 55–59.

[22] L. Liao, Z. Li, T. Lang, and G. Chen, "UV LED array based NLOS UV turbulence channel modeling and experimental verification," *Opt. Exp.*, vol. 23, no. 17, pp. 21825–21835, 2015.

[23] L. C. Andrews and R. L. Phillips, *Laser Beam Propagation Through Random Media*, vol. 152. Bellingham, WA, USA: SPIE, 2005.

[24] W. O. Popoola and Z. Ghassemlooy, "BPSK subcarrier intensity modulated free-space optical communications in atmospheric turbulence," *IEEE/OSA J. Lightw. Technol.*, vol. 27, no. 8, pp. 967–973, Apr. 15, 2009.

[25] A. A. Farid and S. Hranilovic, "Outage capacity optimization for free-space optical links with pointing errors," *J. Lightw. Technol.*, vol. 25, no. 7, pp. 1702–1710, Jul. 2007.

[26] H. Ding, "Modeling and characterization of ultraviolet scattering communication channels," Ph.D. dissertation, Dept. Elect. Eng., UC Riverside, Riverside, CA, USA, 2011.

[27] J. Li, J. Q. Liu, and D. P. Taylor, "Optical communication using subcarrier PSK intensity modulation through atmospheric turbulence channels," *IEEE Trans. Commun.*, vol. 55, no. 8, pp. 1598–1606, Aug. 2007.

[28] X. Zhu and J. M. Kahn, "Free-space optical communication through atmospheric turbulence channels," *IEEE Trans. Commun.*, vol. 50, no. 8, pp. 1293–1300, Aug. 2002.

[29] S. Arya and Y. H. Chung, "M-PSK subcarrier intensity modulation with switch-and-stay diversity for NLOS ultraviolet communication," in *Proc. TENCON IEEE Region Conf.*, Oct. 2018, pp. 0524–0529.

[30] J. C. Ricklin and F. M. Davidson, "Atmospheric turbulence effects on a partially coherent Gaussian beam: Implications for free-space laser communication," *J. Opt. Soc. Amer. A, Opt. Image Sci.*, vol. 19, no. 9, pp. 1794–1802, 2002.

[31] O. Korotkova, S. Avramov-Zamurovic, R. Malek-Madani, and C. Nelson, "Probability density function of the intensity of a laser beam propagating in the maritime environment," *Opt. Exp.*, vol. 19, no. 21, pp. 20322–20331, 2011.

[32] S. Arya and Y. H. Chung, "Generic blind spectrum sensing scheme for all optical-wavelength multi-user free space optical communications," *Opt. Commun.*, vol. 450, pp. 316–321, Nov. 2019.

[33] V. S. Adamchik and O. I. Marichev, "The algorithm for calculating integrals of hypergeometric type functions and its realization in REDUCE system," in *Proc. Int. Symp. Symbolic Algebr. Comput. (ISSAC)*, 1990, pp. 212–224.

[34] A. Jeffrey and D. Zwillinger, *Table of Integrals, Series, and Products*. Amsterdam, The Netherlands: Elsevier, 2007.

[35] S. Z. Denic, I. Djordjevic, J. Anguita, B. Vasic, and M. A. Neifeld, "Information theoretic limits for free-space optical channels with and without memory," *J. Lightw. Technol.*, vol. 26, no. 19, pp. 3376–3384, Oct. 2008.

[36] R. L. Phillips and L. C. Andrews, "Measured statistics of laser-light scattering in atmospheric turbulence," *J. Opt. Soc. Amer.*, vol. 71, no. 12, pp. 1440–1445, 1981.

[37] *The Wolfram Functions Site Wolfram Research, Inc*. Accessed: Mar. 15, 2021. [Online]. Available: http://functions.wolfram.com

[38] S. Arya and Y. H. Chung, "State-of-the-art ultraviolet multiuser indoor communication over power-constrained discrete-time Poisson channels," *Opt. Eng.*, vol. 59, no. 10, Oct. 2020, Art. no. 106106.

[39] Z. Xu, G. Chen, F. Abou-Galala, and M. Leonardi, "Experimental performance evaluation of non-line-of-sight ultraviolet communication systems," *Proc. SPIE*, vol. 6709, Aug. 2007, Art. no. 67090Y.

[40] G. Wang, K. Wang, C. Gong, D. Zou, Z. Jiang, and Z. Xu, "A 1Mbps real-time NLOS UV scattering communication system with receiver diversity over 1km," *IEEE Photon. J.*, vol. 10, no. 2, pp. 1–13, Apr. 2018.

[41] P. Saxena, A. Mathur, and M. R. Bhatnagar, "BER performance of an optically pre-amplified FSO system under turbulence and pointing errors with ASE noise," *IEEE/OSA J. Opt. Commun. Netw.*, vol. 9, no. 6, pp. 498–510, Jun. 2017.

[42] F. Jacobs, "Dependence of optical amplifier noise figure on relative-intensity-noise," *J. Lightw. Technol.*, vol. 13, no. 7, pp. 1461–1465, Jul. 1995.
[43] A. A. M. Saleh, R. M. Jopson, J. D. Evankow, and J. Aspell, "Modeling of gain in erbium-doped fiber amplifiers," *IEEE Photon. Technol. Lett.*, vol. 2, no. 10, pp. 714–717, Oct. 1990.
[44] E. Biglieri, J. Proakis, and S. Shamai (Shitz), "Fading channels: Information-theoretic and communications aspects," *IEEE Trans. Inf. Theory*, vol. 44, no. 6, pp. 2619–2692, Oct. 1998.
[45] A. Garcia-Zambrana, C. Castillo-Vazquez, B. Castillo-Vazquez, and A. Hiniesta-Gomez, "Selection transmit diversity for FSO links over strong atmospheric turbulence channels," *IEEE Photon. Technol. Lett.*, vol. 21, no. 14, pp. 1017–1019, Jul. 2009.
[46] H. E. Nistazakis, T. A. Tsiftsis, and G. S. Tombras, "Performance analysis of free-space optical communication systems over atmospheric turbulence channels," *IET Commun.*, vol. 3, no. 8, pp. 1402–1409, Aug. 2009.
[47] S. Arya and Y. H. Chung, "A unified statistical model for Málaga distributed optical scattering communications," *Opt. Commun.*, vol. 463, May 2020, Art. no. 125402.
[48] B. L. Sharma, "Some formulae for generalized function of two variables," *Matematički Vesnik*, vol. 5, no. 43, pp. 43–52, 1968.
[49] M. Shah, "On generalizations of some results and their applications," *Collectanea Math.*, vol. 24, no. 3, pp. 249–266, 1973.
[50] M. K. Simon and M.-S. Alouini, *Digital Communication Over Fading Channels*, vol. 95. Hoboken, NJ, USA: Wiley, 2005.
[51] *The Mathworks, Inc., Mathworks-MATLAB and Simulink for Technical Computing*. Accessed: Mar. 15, 2021. [Online]. Available: http://www.mathworks.com
[52] I. S. Ansari, S. Al-Ahmadi, F. Yilmaz, M. S. Alouini, and H. Yanikomeroglu, "A new formula for the BER of binary modulations with dual-branch selection over generalized-K composite fading channels," *IEEE Trans. Commun.*, vol. 59, no. 10, pp. 2654–2658, Oct. 2011.
[53] H. Chergui, M. Benjillali, and S. Saoudi, "Performance analysis of project-and-forward relaying in mixed MIMO-pinhole and Rayleigh dual-hop channel," *IEEE Commun. Lett.*, vol. 20, no. 3, pp. 610–613, Mar. 2016.
[54] H. Ding, G. Chen, A. K. Majumdar, and Z. Xu, "A parametric single scattering channel model for non-line-of-sight ultraviolet communications," *Proc. SPIE*, vol. 7091, Aug. 2008, Art. no. 70910M.
[55] G. A. Shaw, A. M. Siegel, and M. L. Nischan, "Demonstration system and applications for compact wireless ultraviolet communications," *Proc. SPIE*, vol. 5071, pp. 241–252, Sep. 2003.

SUDHANSHU ARYA (Member, IEEE) received the M.Tech. degree in communications and networks from the National Institute of Technology, Rourkela, India, in 2017. He is currently pursuing the Ph.D. degree in optical wireless communication with Pukyong National University, Busan, South Korea. His research interests include wireless communications and digital signal processing with focus has been placed on free-space optical communications, optical scattering communications, optical spectrum sensing, computational game theory, and artificial intelligence. He received the Best Paper Award in ICGHIT 2018. He also received the Early Career Researcher Award from Pukyong National University, in 2020.

YEON HO CHUNG (Senior Member, IEEE) received the M.Sc. degree from Imperial College London, U.K., in 1992, and the Ph.D. degree from the University of Liverpool, U.K., in 1996. He was a Visiting Professor with Pennsylvania State University, University Park, PA, USA, and also with Chiba University, Japan. He is currently a Professor with the Department of Information and Communications Engineering, Pukyong National University, Busan, South Korea. He was a Foreign Expert for the GIAN Program of the Government of India, in 2017. He was a Keynote Speaker for IFIP WMNC 2018 and CSNDSP 2020. His research interests include visible light communications, optical camera communications, optical scattering communications, optical healthcare systems, and advanced wireless transmission schemes. He is also a member of the Editorial Board of the *International Journal of Wireless Personal Communications* (Springer). He received the Top 2014 Paper Award from *Transactions on Emerging Telecommunications Technologies* (ETT) (Wiley) and the Best Paper Award from ICUFN 2019. He also received the Busan Science and Technology Award for outstanding research achievements. He is also the Editor-in-Chief of *International Journal of Sensors, Wireless Communications and Control* (Bentham Science Publishing). He is also an Associate Editor of IEEE Access.